

Top-Quark Mediated Effects in Hadronic Higgs-Strahlung

Oliver Brein^a, Robert V. Harlander^b, Marius Wiesemann^b, Tom Zirke^b

^a *Physikalisches Institut, Albert-Ludwigs-Universität Freiburg,
D-79104 Freiburg i.Br, Germany*

^b *Fachbereich C, Bergische Universität Wuppertal,
42097 Wuppertal, Germany*

Abstract

Novel contributions to the total inclusive cross section for Higgs-Strahlung in the Standard Model at hadron colliders are evaluated. Although formally of order α_s^2 , they have not been taken into account in previous NNLO predictions. The terms under consideration are induced by Higgs radiation off top-quark loops and thus proportional to the top-quark Yukawa coupling. At the Tevatron, their effects to WH production are below 1% in the relevant Higgs mass range, while for ZH production, we find corrections between about 1% and 2%. At the LHC, the contribution of the newly evaluated terms to the cross section is typically of the order of 1%-3%. Based on these results, we provide updated predictions for the total inclusive Higgs-Strahlung cross section at the Tevatron and the LHC.

1 Introduction

With the LHC experiments becoming sensitive to signals for the Standard Model (SM) Higgs boson, the search for this elusive particle has entered a new and hopefully its final phase. The direct searches at LEP, Tevatron, and LHC only leave relatively small allowed windows for the Higgs mass M_H , the widest one between 114 GeV and about 145 GeV (see Ref. [1,2] for preliminary results).

As opposed to evidence or discovery, the exclusion limits rely heavily on theoretical predictions. The dominant cross section to compare the experimental measurements to is gluon fusion which receives large radiative corrections. Although it is probably the most-studied cross section for an unconfirmed particle, the residual theoretical uncertainty is still sizable and highly disputed (for a recent discussion, see Ref. [3]). A lot of this uncertainty is induced by quantum chromodynamics (QCD), specifically the strong coupling α_s and the parton density functions (PDFs).

For various reasons, however, gluon fusion need not be the dominant search mode. The focus of this paper is on the associated production of a Higgs boson with an electro-weak

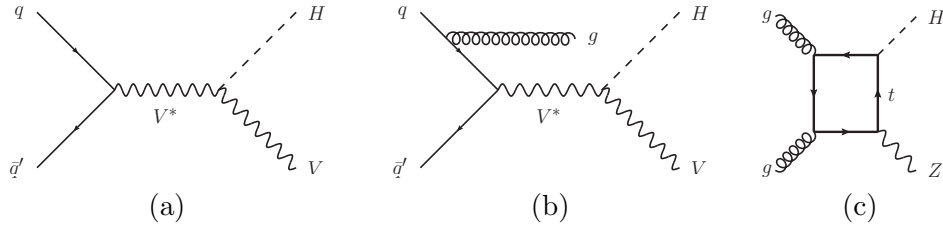


Figure 1: (a) Leading order Feynman diagram contributing to the Higgs-Strahlung process; (b) real corrections at NLO QCD; (c) gg component not covered by Drell-Yan-like corrections.

gauge boson ($pp \rightarrow VH$, $V \in \{W^\pm, Z\}$), or “Higgs-Strahlung” for short. At the Tevatron, where the $\gamma\gamma$ and $b\bar{b}$ -decays of a Higgs boson produced in gluon fusion cannot be separated from the background with sufficient precision, this mode is particularly important in the low mass region. Nominally known through order α_s^2 , we identify and evaluate a previously neglected contribution which formally adds to these next-to-next-to-leading order (NNLO) terms.

For the LHC, the relevance of the Higgs-Strahlung process used to be considered marginal. This has changed with the idea of focusing on events with highly boosted Higgs bosons by analyzing the substructure of jets [4]. Even though for a proper theoretical prediction in such an analysis one needs to consider differential quantities, it is important to ensure that all effects that contribute to the total rate are under control.

Once the Higgs mass is known, precise predictions for the individual production and decay channels will be essential in order to extract the maximum information from the experiments (see, e.g., Ref. [5]).

The theoretical prediction of the total inclusive cross section due to Higgs-Strahlung at hadron colliders is under very good control¹: the leading order contribution is of order g^4 , where g is the weak coupling constant, and is completely analogous to what used to be the main search channel at LEP, except that the initial e^+e^- is replaced by a $q\bar{q}'$ pair, of course, see Fig. 1 (a). The NLO QCD [7] and the bulk of the NNLO QCD corrections [8], i.e. $\mathcal{O}(g^4\alpha_s)$ and $\mathcal{O}(g^4\alpha_s^2)$, can be reduced to the Drell-Yan production of a virtual gauge boson [9, 10]. The theoretical uncertainty due to PDFs has been estimated to be at the percent level, and the renormalization/factorization scale dependence of these terms is practically negligible [11]. For ZH production at $\mathcal{O}(\alpha_s^2)$, however, there are a few classes of diagrams that have no correspondence to the Drell-Yan process. For example, the gluon-induced virtual corrections mediated by a top-quark loop are of order $g^2\lambda_t^2\alpha_s^2$ (see Fig. 1 (c)), where λ_t is the top-quark Yukawa coupling which, in the SM, is of order one. These corrections were evaluated in Refs. [8, 12] and found to be of the order of 5% at the

¹For recent work on higher order differential WH cross sections, see Ref. [6].

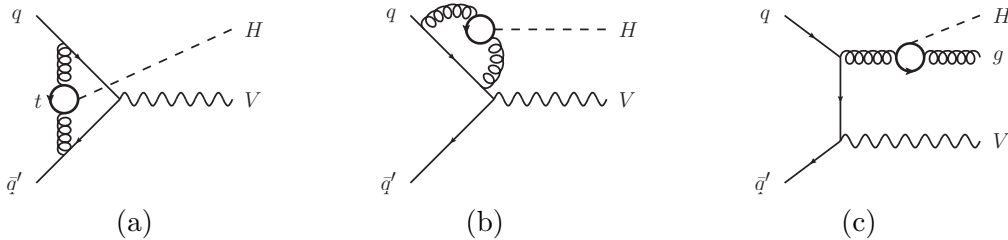


Figure 2: (a),(b) Diagrams of group V_I and (c) group R_I contributing to the process $q\bar{q} \rightarrow VH(g)$ at order $g^3\lambda_t\alpha_s^2$.

LHC.

In this paper we consider another class of diagrams which are formally of order $g^3\lambda_t\alpha_s^2$ and were neglected in previous analyses. For simplicity, we will refer to them as “top-mediated terms” in this paper, even though they are not the only contributions involving top-quarks, as noted above. Their numerical impact is at the percent level and therefore within the *current* estimated theoretical uncertainty of the NNLO result (see Ref. [11]). Note, however, that this uncertainty estimate is dominated by the effects from PDFs and α_s ; once these will be known with higher precision, the results of this paper will be required for the perturbative part to compete with this precision.

The remainder of this paper is organized as follows: Section 2 defines the effects to be calculated, briefly describes the methods applied, and presents analytical expressions for part of the results. In Section 3, we study the size of the newly evaluated effects and present updated values for the total inclusive cross section for WH and ZH production at the Tevatron and the LHC at collision energies of 7 and 14 TeV.

2 Computational details

2.1 Outline of the problem

The Feynman diagrams of the top-mediated terms considered in this paper can be divided into four groups which will be described in this section.

Examples of diagrams of the first group, named V_I in what follows, are shown in Fig. 2 (a) and (b). They are characterized by the emission of a Higgs boson off a top-quark bubble-insertion into an *internal* (i.e. virtual) gluon line. They contribute to the total cross section through the interference with the leading order amplitude (see Fig. 1 (a)).

The second group (R_I), see Fig. 2 (c), can be viewed as the real emission counterpart of group V_I . It is obtained by radiating the Higgs off a top-quark bubble-insertion into an

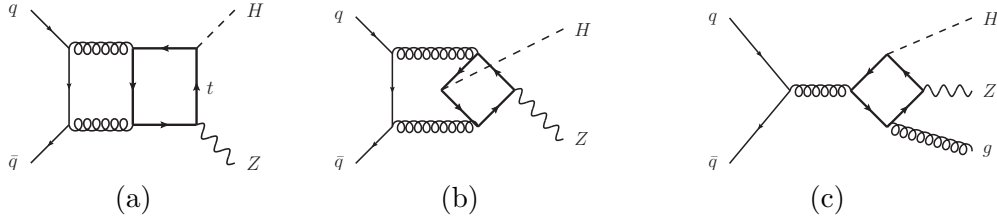


Figure 3: (a),(b) Diagrams of group V_{II} and (c) group R_{II} contributing to the process $q\bar{q} \rightarrow ZH(g)$ at order $g^3\lambda_t\alpha_s^2$.

external gluon line. These diagrams have to be interfered with the real-emission amplitude contributing to the NLO QCD cross section, see Fig. 1 (b). Needless to say that the crossed amplitudes, where the gluon is in- and a quark or anti-quark is out-going, have to be taken into account as well.

The third group of Feynman diagrams (V_{II}) is closely related to the gluon-induced contribution of Fig. 1 (c). While the latter enters the total cross section with its square, the new contributions treated here are genuine two-loop terms which are to be interfered with the tree-level amplitude of Fig. 1 (a). Examples are shown in Fig. 3 (a) and (b). Finally, the fourth group (R_{II}) can again be seen as the real-emission counterpart of group V_{II} . An example is shown in Fig. 3 (c). Also here, of course, one can cross the gluon and the quark or anti-quark from the final to the initial state and vice versa.

The amplitude for each of these groups is separately gauge invariant and UV- as well as IR-finite, despite the fact that two of them can each be viewed as real and virtual correspondences of each other.

The diagrams of R_{I} and R_{II} can be calculated exactly, taking into account the full dependence on the top, Higgs, and vector boson mass. The amplitude arising from groups V_{I} and V_{II} , on the other hand, is very challenging to compute and may be even beyond current technology. We therefore follow the established and successful method of asymptotic expansions in order to approximate the result in the limit of infinite top-quark mass M_t . The validity of this approach will be discussed below.

In a fully consistent treatment of the contributions described in this section, one needs to take into account yet another set of Feynman diagrams. They can be obtained from the previous ones by radiating the Higgs boson off the external vector boson instead of the top-quark loop, see Fig. 4, for example.² If all couplings are replaced by their SM values, the resulting amplitudes are of the same perturbative order as the ones discussed in this paper; however, they receive an additional suppression factor $\sim M_V^2/(\hat{s} - M_V^2)$, where M_V is the mass of the vector boson and $\sqrt{\hat{s}} \geq M_V + M_H$ the partonic center-of-mass

²Due to the requirement of anomaly cancellation, however, they have to be supplemented by triangle diagrams with bottom- instead of top-quarks running in the loop.

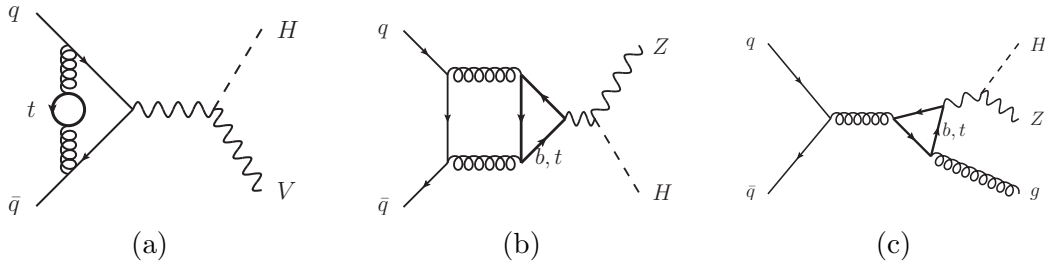


Figure 4: Drell-Yan-like diagrams with closed top- and bottom-quark loops.

energy. Justifiably so, these terms have been considered Drell-Yan-like in Ref. [8]; in fact, they can be calculated by convolving the output of (a suitably modified version of) the program MASSIVE [13] with the decay $V^* \rightarrow VH$. As a check, we also calculated some of these contributions directly using the methods described below. The result confirms the statement of Refs. [8, 12] that these contributions are numerically irrelevant: they are typically 2-3 orders of magnitude smaller than the other newly evaluated contributions considered in this paper, and will therefore be neglected in what follows.

2.2 Calculation of V_I and V_{II}

A priori, an expansion of the two-loop amplitudes in the limit of large top-quark mass seems unjustified, because the partonic center of mass energy $\sqrt{\hat{s}}$ at the Tevatron and the LHC can be much larger than M_t (or rather $2M_t$ which corresponds to the threshold and is thus the relevant scale). Nevertheless, there is a number of arguments that make such an approach reasonable, if M_H is not too large:

- The parton luminosities at large \hat{s} are strongly suppressed, and the bulk of the contribution to the total cross section indeed arises from the region below the top-quark threshold. This is similar to what happens in the case of gluon fusion, see Refs. [14–16]. For Higgs-Strahlung, however, the situation is somewhat worse, because the energy window for which the heavy-top expansion is expected to converge is much narrower than for gluon fusion: $M_V + M_H \leq \sqrt{\hat{s}} \leq 2M_t$. In fact, for $M_H \gtrsim 250$ GeV, this restriction cannot be obeyed at all.
- For group V_I (Fig. 2 (a),(b)), the typical energy scale affecting the top-quark loop is not the full center-of-mass energy, but significantly below that, because the vector boson carries off a large fraction of the momentum.
- Since group V_{II} (Fig. 3 (a),(b)) is closely related to the gg -induced contribution of Fig. 1 (c), we may estimate its impact by the ratio of the $q\bar{q}$ and the gg luminosity

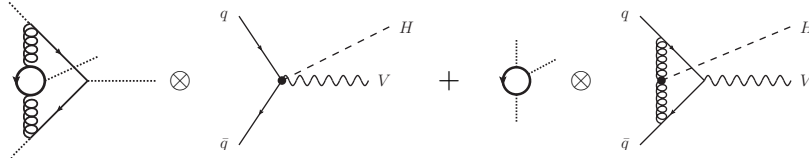


Figure 5: Asymptotic expansion of the diagram in Fig. 2 (a). The diagrams left of \otimes are evaluated after setting their external momenta to zero. The result determines the expression to be inserted into the effective $\bar{q}qVH$ or ggH vertex in the diagram right of \otimes . For details on the general method, see Refs. [29–31], for example.

times the gg -induced cross section. It should therefore not exceed a few percent of the LO cross section.

- Overall, we expect the top-mediated terms to affect the cross section at the percent level [6, 17]. The leading term of an expansion in terms of $1/M_t$ should thus be sufficiently precise.

The tools to calculate the diagrams are by now standard: asymptotic expansion of the two-loop diagrams of groups V_I and V_{II} leads to a factorization of scales into either two-loop massive tadpoles (i.e., vanishing external momenta) times tree-level diagrams with an effective $\bar{q}qH$ or $\bar{q}qVH$ vertex, or one-loop massive tadpoles times massless one-loop diagrams with an effective $ggZH$ or ggH vertex. As an example, the graphical representation of the asymptotic expansion of the diagram in Fig. 2 (a) is shown in Fig. 5.

We use the automatic setup consisting of `qgraf` [18] for the generation, and `q2e/exp` [19,20] for the expansion of the diagrams, as well as `MATAD` [21] for the calculation of the tadpole integrals. In order to evaluate the massless one-loop box and triangle integrals corresponding to the right-most diagrams in Fig. 5, we supplement this setup by an additional routine (based on `FORM` [22]) which implements standard Passarino-Veltman reduction [23] in algebraic form. The scalar one-loop Feynman integrals are evaluated using the results of Ref. [24].

It turns out that for V_I , the sum of terms involving an effective $\bar{q}qVH$ or $\bar{q}qH$ vertex does not contribute at leading order in $1/M_t$, i.e., the corrections can be calculated by simply using an effective ggH vertex and evaluating one-loop diagrams. This observation allowed us to obtain V_I in a second, independent calculation by using a generalized version of the `FORM` program `FDiag` [25] and the Fortran package `FF` [26–28], supplemented by a routine to facilitate the tensor reduction of rank-4 tensor 4-point functions and the subsequent numerical evaluation of the corresponding tensor coefficients.

Contracting with the LO amplitude and summing/averaging over final/initial color and spin degrees of freedom, we find for the amplitude of V_I , cf. Fig. 2 (a),(b):

$$\begin{aligned}
-\frac{d\Delta\hat{\sigma}_I^V}{d\hat{t}} &= G_{qq'}^V \frac{G_F^2 M_V^4}{108\pi\hat{s}^2(\hat{s} - M_V^2)} \left(\frac{\alpha_s}{\pi}\right)^2 \text{Re} \left\{ -2\hat{s} \right. \\
&\quad + \ln\left(\frac{\hat{u}}{M_V^2}\right) \left(\hat{t} - M_V^2 + \frac{2\hat{s}M_V^2}{\hat{u} - M_V^2}\right) + \ln\left(\frac{\hat{t}}{M_V^2}\right) \left(\hat{u} - M_V^2 + \frac{2\hat{s}M_V^2}{\hat{t} - M_V^2}\right) \\
&\quad + (\hat{s} - M_H^2 + M_V^2) \left[\ln^2\left(\frac{\hat{t}}{\hat{u}}\right) + 2\text{Li}_2\left(1 - \frac{M_H^2}{\hat{t}}\right) + 2\text{Li}_2\left(1 - \frac{M_H^2}{\hat{u}}\right) \right. \\
&\quad \left. + 2\text{Li}_2\left(1 - \frac{M_V^2}{\hat{t}}\right) + 2\text{Li}_2\left(1 - \frac{M_V^2}{\hat{u}}\right) - 2\text{Li}_2\left(1 - \frac{M_H^2 M_V^2}{\hat{t}\hat{u}}\right) \right] + \mathcal{O}\left(\frac{1}{M_t^2}\right) \left. \right\}, \tag{1}
\end{aligned}$$

where $\hat{s} = (p_1 + p_2)^2$, $\hat{t} = (p_1 - p_V)^2$ and $\hat{u} = (p_1 - p_H)^2$ are the usual (partonic) Mandelstam variables, with the incoming momenta p_1, p_2 , and p_H, p_V the momenta of the Higgs and the vector boson, respectively. M_V is the mass of the emitted vector boson, and Li_2 denotes the di-logarithm. The electro-weak couplings are given by

$$\begin{aligned}
G_{qq'}^Z &= (v_q^2 + a_q^2)\delta_{qq'}, \quad G_{qq'}^W = \frac{1}{2}|V_{qq'}|^2, \\
v_q &= \pm\frac{1}{2} + \frac{1}{3} \left\{ \begin{array}{c} -4 \\ +2 \end{array} \right\} \sin^2\theta_W, \quad a_q = \pm\frac{1}{2} \quad \text{for } q \in \left\{ \begin{array}{c} u, c \\ d, s, b \end{array} \right\}, \tag{2}
\end{aligned}$$

with the weak mixing angle $\sin^2\theta_W = 1 - M_W^2/M_Z^2$ and the CKM matrix elements $V_{qq'}$ (see Ref. [32] for the latest numerical values; we set $V_{qq'} = 0$ if both q and q' carry the same weak isospin charge I_3). We have expressed the top-quark Yukawa coupling by the tree-level relation

$$\lambda_t \equiv \frac{M_t}{v} = M_t \sqrt{\sqrt{2}G_F} \tag{3}$$

in Eq. (1), and also in Eq. (6) below. Similar to the gluon fusion process, the factor M_t cancels against its inverse from the top-loop integration.

For group V_{II} (see Fig. 3 (a),(b)), only the axial vector part of the Z coupling to fermions contributes. We implement its Dirac structure with the help of Levi-Civita symbols $\varepsilon_{\mu\nu\rho\sigma}$ [33]

$$\gamma_\mu \gamma_5 \rightarrow \frac{i}{3!} \varepsilon_{\mu\alpha\beta\delta} \gamma^\alpha \gamma^\beta \gamma^\delta, \tag{4}$$

and re-write their product in terms of the anti-symmetrized (denoted by square brackets) D -dimensional metric tensor,

$$\varepsilon_{\mu\nu\rho\sigma} \varepsilon^{\alpha\beta\gamma\delta} = -g_{[\mu}^{\alpha} g_{\nu}^{\beta} g_{\rho}^{\gamma} g_{\sigma]}^{\delta]}. \tag{5}$$

Upon asymptotic expansion of the diagrams, the terms corresponding to an effective $ggZH$ vertex contribute only at subleading order in $1/M_t$, and the calculation reduces to massive 2-loop tadpole diagrams.

The result assumes the simple form

$$-\frac{d\Delta\hat{\sigma}_{\text{II}}^Z}{d\hat{t}} = \frac{G_{\text{F}}^2 M_Z^4 a_t a_q}{12\pi\hat{s}^2(\hat{s} - M_Z^2)} \left(\frac{\alpha_s}{\pi}\right)^2 \left\{ 2\hat{s} - M_H^2 + \frac{\hat{t}\hat{u}}{M_Z^2} + \mathcal{O}\left(\frac{1}{M_t}\right) \right\}. \quad (6)$$

Since the expressions in Eq. (1) and (6) are free of divergences in the allowed \hat{t} -region, we can numerically integrate them together with the convolutions over the PDFs in order to get their contribution to the total inclusive hadronic cross section. The numerical results will be presented in the next section.

2.3 Calculation of R_{I} and R_{II}

Being of one-loop order, the diagrams of groups R_{I} and R_{II} can be calculated including the full dependence on the top-quark, Higgs- and vector-boson mass by means of Passarino-Veltman reduction to scalar one-loop functions. In most of the phase-space, the numerical evaluation of these function can be performed with the help of the programs `FDiag` and `FF` (see Sec. 2.2), and independently with `FeynArts`, `FormCalc`, and `LoopTools` [34] (the latter of which relies on `FF` though). The contribution R_{II} , however, involves momentum configurations that are outside `FF`'s capabilities. For those, we use an implementation of the one-loop integrals based on Refs. [35, 36]³. Again, since projection with the LO amplitude leads to a finite expression, phase-space integration and convolution with PDFs can be done fully numerically.

2.4 Validation of the heavy-top approximation

This section describes both a consistency check for our calculation of the real-emission contributions R_{I} and R_{II} , as well as a validity check of our approach to the virtual terms V_{I} and V_{II} .

In addition to the exact calculation as described in Section 2.3, we evaluated the real emission amplitudes R_{I} and R_{II} also by applying asymptotic expansions in the heavy-top limit. In these cases, it reduces to a naive Taylor expansion of the integrand before loop integration. We can again perform all phase-space integrals numerically. In the $q\bar{q}$ -channel, however, we also integrated over the angular variables of the phase-space analytically in $D = 4 - 2\epsilon$ space-time dimensions, and found the cancellation of all poles at $\epsilon = 0$. The numerical integration over the remaining energy variables is straightforward and leads to the same result as the all-numerical method.

³We thank Stefan Dittmaier for providing us with his private code.

Comparing this heavy-top result for R_{I} and R_{II} at the partonic level to the exact results described above, we indeed observe that heavy-top limit systematically approaches the exact result as $\mathcal{E}/M_t \rightarrow 0$, where \mathcal{E} is any of the external energy scales. In particular, we observe that, as opposed to the other contributions, the terms R_{II} vanish as $1/M_t^2$ in the limit $M_t \rightarrow \infty$. This agreement between the exact and the asymptotic approach provides a strong and valuable check on our results.

In order to draw conclusions for the validity of the heavy-top expansion, however, the relevant quantity to compare is the hadronic cross section, of course. For that, we find that the heavy-top result is roughly within 25%/35% of the full result at the LHC/Tevatron in the mass range considered in this paper.

We expect a similar quality of the heavy-top result for the contributions from V_{I} and V_{II} . To be conservative, we attribute an additional uncertainty of 30%/50% (relative to the central values) to these terms for the LHC/Tevatron prediction of the hadronic cross section.

3 Numerics

3.1 Size of the top-induced terms

We present numbers for the Tevatron ($p\bar{p}$ @ $\sqrt{s} = 1.96$ TeV), as well as the LHC (pp @ 7 TeV and 14 TeV). The hadronic cross section is evaluated by folding the partonic cross section with PDFs. Although the corrections evaluated in this paper are not renormalized by lower order terms, we think it is appropriate to convolve them with NNLO PDFs. We use the central MSTW2008 set, implying $\alpha_s(M_Z) = 0.1171$. For the physical parameters, we assume the values

$$M_Z = 91.1876 \text{ GeV}, \quad M_W = 80.398 \text{ GeV}. \quad (7)$$

Since the amplitudes considered in this paper are UV- and IR-finite, they do not depend explicitly on the renormalization or factorization scale ($\mu_{\text{R}}, \mu_{\text{F}}$). However, these scales enter implicitly through the strong coupling and the PDFs. For the numerical analysis, we choose

$$q^2 \equiv (p_H + p_V)^2$$

as the central scale for μ_{R}^2 and μ_{F}^2 , where p_H and p_V are the 4-momenta of the Higgs and the outgoing vector boson. For the Drell-Yan-like terms, $\sqrt{q^2}$ equals the invariant mass of the intermediate gauge boson. In order to estimate the theoretical uncertainty of our results, we vary μ_{R} by a factor of three around this central scale while keeping μ_{F} fixed,

$$\frac{1}{3}\sqrt{q^2} \leq \mu_{\text{R}} \leq 3\sqrt{q^2}, \quad \mu_{\text{F}} = \sqrt{q^2}, \quad (8)$$

then repeat the analysis after interchanging μ_F and μ_R , and take the extreme values of the cross section as uncertainty band.

Fig. 6 shows the contribution of the newly evaluated terms to the total inclusive cross sections $\sigma(pp \rightarrow WH) \equiv \sigma(pp \rightarrow W^+H) + \sigma(pp \rightarrow W^-H)$ and $\sigma(pp \rightarrow ZH)$ at 7 TeV and 14 TeV center-of-mass energy. The contributions from the various groups of diagrams (see Section 2.1) are shown separately, each of them with an error band derived from the scale variation described above. Also shown is the sum of all contributions. The corresponding plots for the Tevatron are shown in Fig. 7.

The size of the V_I component amounts to about 0.5% of the LO cross section⁴ both for WH and ZH production, independent of collider type, center-of-mass energy, and Higgs boson mass. While at the LHC the R_I terms are typically a little larger than that, and increase with M_H and the center-of-mass energy, they always remain below 0.5% at the Tevatron.

Since V_I and R_I are the only non-vanishing contributions for WH production, in this case the overall effect of the top-mediated terms evaluated in this paper remains below 1% at the Tevatron, and ranges between about 1.1% (for $M_H = 100$ GeV at 7 TeV) to 2.4% (for $M_H = 300$ GeV at 14 TeV) at the LHC (see Fig. 6 (a) and Fig. 7 (a)).

For ZH production, also the groups V_{II} and R_{II} have to be taken into account. Being suppressed by $1/M_t^2$ at large M_t , as pointed out above, the terms R_{II} have only a very small numerical impact at the per-mille level. The relative contribution of V_{II} , on the other hand, increases with the Higgs boson mass, but remains below 0.8% at the LHC in all of the considered Higgs mass range. At the Tevatron, however, it exceeds V_I and R_I above $M_H \approx 130$ GeV and ranges up to about 1% at $M_H = 200$ GeV. The overall effect of V_I , R_I , V_{II} , and R_{II} on ZH production at the Tevatron is therefore between 1% and 2%, while it ranges between 1.1% (for $M_H = 100$ GeV at 7 TeV) and 2.9% (for $M_H = 300$ GeV at 14 TeV) at the LHC (see Fig. 6 (b) and Fig. 7 (b)).

In each case, a rough estimate of the uncertainty on the top-mediated terms due to scale variation is 20-30%. As discussed in Section 2.4, we also include an estimated uncertainty on the V_I and V_{II} terms of 30%/50% for the LHC/Tevatron, arising from the heavy-top limit (this is not included in Figs. 6 and 7). Considering the fact that the corrections are at the percent level, this uncertainty will affect the accuracy of the total inclusive cross section by roughly 0.5%. We do not expect the PDF uncertainties on the top-induced terms to add significantly to the one of the total cross section and will neglect it in what follows.

⁴Only central values are considered in this discussion.

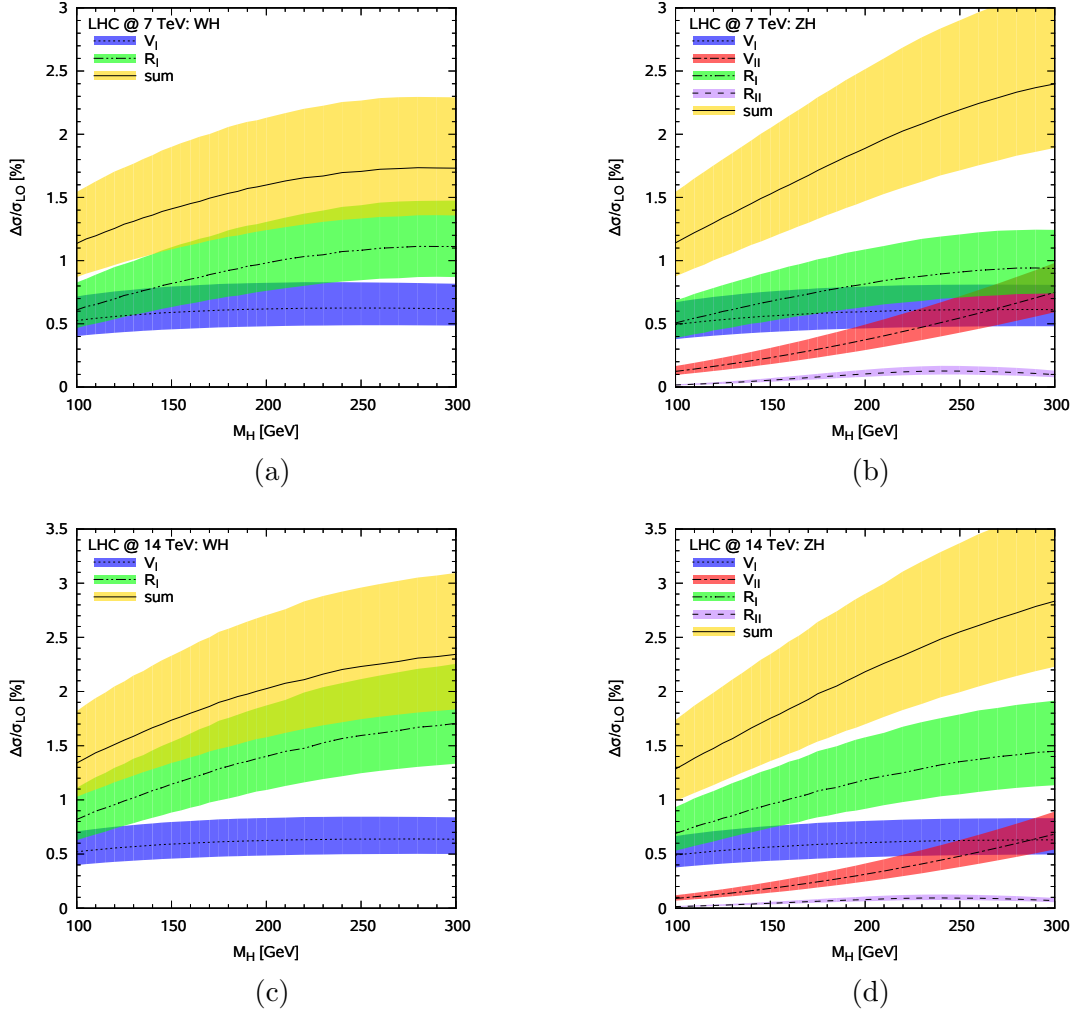


Figure 6: Contribution of the corrections evaluated in this work to the total inclusive cross section $\sigma(pp \rightarrow WH + X)$ (left column) and $\sigma(pp \rightarrow ZH + X)$ (right column) at the LHC with 7 TeV (upper row) and 14 TeV center-of-mass energy (lower row). The effects are shown relative to the leading order cross section σ_{LO} . The various bands show the contributions from V_I , R_I , and, in the case of ZH , V_{II} and R_{II} . The upper band is the sum of all contributions. The width of the band arises from the variation of μ_R and μ_F as described in the main text.

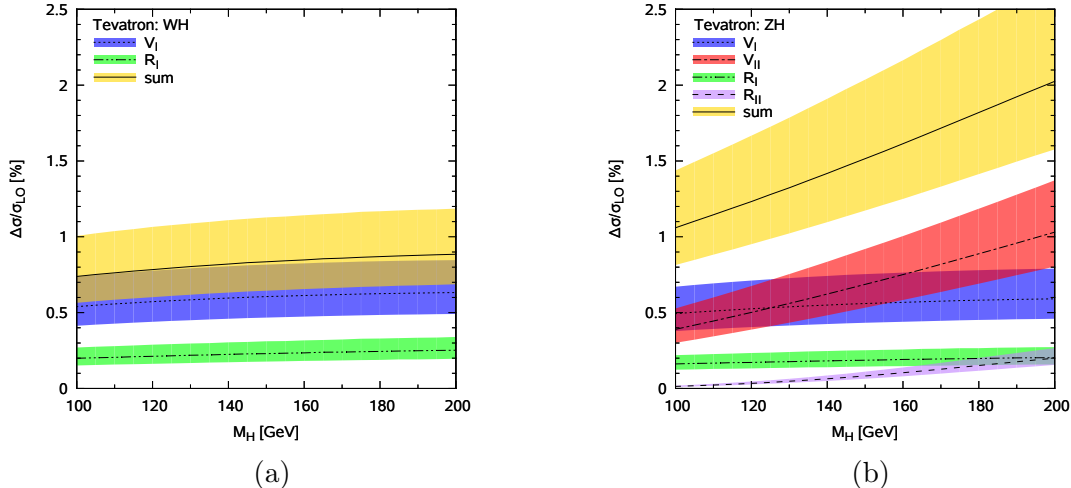


Figure 7: Same as Fig. 6, but for WH/ZH production at the Tevatron.

3.2 Total inclusive cross section

As shown in the previous section, the effects of the newly evaluated terms are of the order of 1-3% of the LO cross section on WH and ZH production. Superficially, this lies within previous estimates of the uncertainties of the total inclusive cross section at the LHC [11]. However, most of this uncertainty is induced by the PDFs. Once systematical effects and theoretical ambiguities will have been settled (for a recent discussion, see Ref. [3]) or become irrelevant due to the inclusion of LHC data, one may expect these uncertainties to shrink significantly. Then, in order to arrive at the most precise prediction for the process, the effects of the top-mediated terms evaluated here will have to be included.

For this reason, we provide an updated prediction of the total inclusive cross section for WH and ZH production at the Tevatron and the LHC at 7 TeV and 14 TeV in this section. The numbers for the LHC are obtained simply by adding the top-mediated terms to the predictions of Ref. [11], which have been obtained using the program `vh@nnlo` [37], based on the calculation of Refs. [8–10] and the program `zwprod` [9], and an electro-weak correction factor [38]. The uncertainties on the numbers given here result from linearly adding the previous uncertainties [11] to the ones discussed in Section 3.1.

For the Tevatron, an “official” public agreement on the cross section prediction analogous to Ref. [11] is not available. We therefore follow the analysis of Ref. [11] using Tevatron parameters, and proceed as above. The electro-weak correction factor we read off from the plots and tables of Ref. [38] in this case, despite the fact that the parameters in this paper are slightly outdated. The uncertainty induced by this procedure should be negligible, however.

The final results are presented in Tables 1, 2, and 3 for the LHC at 7 TeV, 14 TeV, and the Tevatron, respectively. The top-mediated terms slightly increase all the cross sections, but also the theoretical uncertainty. The column labeled “Pert” in the tables contains the estimate of the perturbative uncertainty as described in Section 3.1. The column labeled “PDF+ α_s ” displays the error induced by the PDFs and the input value for α_s , as described in Ref. [11].

Finally, Figs. 8 and 9 show the K-factors resulting from our compilation, including NNLO QCD, electro-weak effects, and the newly evaluated top-mediated terms of this paper. In the LHC case, we also show the previous numbers from Ref. [11], and for the Tevatron we provide the analogous numbers with the same input data.

These plots clearly show that for the LHC, the top-mediated terms affect the WH production cross section at the order of the estimated perturbative uncertainties. In fact, note that for $\sqrt{s} = 14$ TeV and above around $M_H = 160$ GeV, the uncertainty bands of the predictions with and without the top-induced terms hardly overlap. Since the uncertainty bands of the ZH channel are significantly larger than for WH , mostly due to the gg -induced terms of Fig. 1 (c), the relative importance of the top-mediated terms on ZH is much smaller than for WH .

At the Tevatron, the K-factor is typically larger than at the LHC, and the top-mediated terms have a rather small impact. Also, the difference between WH and ZH in the K-factor is much less pronounced than at the LHC, the reason being again the gg -induced terms which have much smaller impact at the Tevatron.

4 Conclusions and Outlook

The effects of an as of yet neglected contribution to the Higgs-Strahlung process at hadron colliders have been studied. The relevant Feynman diagrams contain closed top-quark loops and are of order $g^3 \lambda_t \alpha_s^2$. The one-loop real-emission contributions were evaluated exactly, while the two-loop virtual terms were evaluated in the heavy-top limit. It was argued that this provides a reliable approximation to the exact result. The numerical impact of the newly evaluated terms is within the current estimate for the theoretical uncertainty, but may well become important once the uncertainty induced by PDFs and the strong coupling reduces.

We plan to include the newly evaluated terms in the publicly available program `vh@nnlo` in order to provide a tool for the evaluation of the the full $\mathcal{O}(\alpha_s^2)$ prediction for ZH and WH production.

Finally, let us remark that similar contributions exist also for the weak-boson fusion process [39–42]. Parts of them were evaluated in Ref. [43].

M_H [GeV]	$\sigma(WH)$ [fb]	Pert [%]	PDF+ α_s [%]	$\sigma(ZH)$ [fb]	Pert [%]	PDF+ α_s [%]
100	1197	+1.0 -0.8	± 3.4	636.8	+1.5 -1.5	± 3.4
105	1027	+0.8 -1.1	± 3.5	549.8	+1.7 -1.9	± 3.7
110	883.7	+0.7 -1.0	± 3.8	476.5	+1.6 -1.6	± 4.1
115	762.0	+0.8 -1.1	± 3.9	414.6	+1.7 -1.5	± 4.2
120	662.7	+0.8 -1.1	± 3.4	363.3	+2.0 -1.6	± 3.5
125	578.8	+0.6 -1.2	± 3.5	319.0	+1.9 -2.0	± 3.5
130	506.1	+0.8 -1.1	± 3.5	280.7	+2.0 -1.8	± 3.7
135	443.7	+1.1 -0.8	± 3.4	247.9	+2.2 -1.8	± 3.6
140	389.9	+1.0 -0.9	± 3.5	219.5	+2.0 -2.0	± 3.7
145	344.4	+0.7 -1.1	± 3.8	195.2	+2.3 -2.2	± 4.0
150	303.5	+0.9 -1.1	± 3.3	173.2	+2.3 -2.0	± 3.6
155	267.7	+1.0 -1.1	± 3.5	154.3	+2.6 -2.0	± 3.6
160	231.9	+1.0 -1.1	± 3.8	135.0	+2.5 -2.1	± 4.0
165	213.2	+1.0 -1.1	± 3.6	124.8	+2.7 -2.1	± 4.1
170	190.7	+1.0 -1.1	± 3.8	112.0	+2.7 -2.3	± 4.2
175	171.0	+0.8 -1.5	± 3.8	100.8	+2.7 -2.3	± 4.1
180	154.0	+1.1 -1.0	± 3.5	90.34	+2.8 -2.3	± 3.8
185	140.5	+0.9 -1.2	± 3.5	82.46	+2.9 -2.4	± 3.8
190	126.9	+1.1 -1.1	± 3.7	74.65	+2.8 -2.6	± 3.9
195	115.2	+1.2 -1.0	± 3.7	67.91	+2.9 -2.4	± 4.0
200	104.6	+0.9 -1.3	± 3.8	61.81	+2.9 -2.4	± 4.1
210	86.70	+1.0 -1.1	± 3.7	51.41	+2.8 -2.5	± 4.2
220	72.38	+0.9 -1.3	± 3.7	42.97	+2.9 -2.4	± 4.2
230	60.87	+1.3 -1.1	± 4.5	36.15	+2.8 -2.4	± 4.8
240	51.45	+1.1 -1.2	± 4.0	30.46	+2.6 -2.4	± 4.4
250	43.68	+1.1 -1.1	± 4.0	25.81	+2.7 -2.2	± 4.2
260	37.25	+1.3 -1.1	± 4.0	21.94	+2.6 -2.3	± 4.5
270	31.91	+1.2 -1.3	± 3.8	18.70	+2.4 -2.2	± 4.3
280	27.39	+0.9 -1.4	± 4.4	16.02	+2.4 -1.9	± 4.9
290	23.65	+1.2 -1.2	± 4.2	13.79	+2.3 -2.0	± 4.5
300	20.47	+1.1 -1.3	± 4.5	11.90	+2.2 -1.8	± 5.0

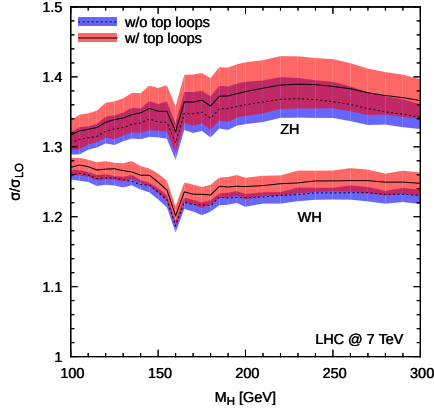
Table 1: Numerical values for the total cross section at LHC at 7 TeV.

M_H [GeV]	$\sigma(WH)$ [fb]	Pert [%]	PDF+ α_s [%]	$\sigma(ZH)$ [fb]	Pert [%]	PDF+ α_s [%]
100	3035	+1.3 -0.9	± 3.7	1700	+2.3 -1.9	± 3.8
105	2625	+1.1 -0.8	± 3.5	1483	+2.2 -2.1	± 3.7
110	2273	+0.8 -1.1	± 3.8	1297	+2.6 -2.0	± 4.0
115	1976	+1.2 -0.6	± 3.8	1142	+2.9 -1.9	± 3.7
120	1731	+1.1 -0.7	± 3.8	1008	+2.9 -2.2	± 3.6
125	1523	+0.9 -1.0	± 3.8	893.2	+3.2 -2.2	± 3.7
130	1342	+1.0 -0.8	± 3.3	793.9	+3.4 -2.2	± 3.4
135	1183	+1.2 -0.9	± 2.9	706.6	+3.4 -2.6	± 3.0
140	1048	+0.8 -1.1	± 3.1	633.4	+3.4 -2.6	± 3.0
145	933.1	+1.1 -0.8	± 3.3	567.2	+3.8 -2.5	± 3.4
150	827.5	+0.9 -1.1	± 2.7	508.2	+3.8 -2.4	± 2.7
155	736.3	+0.9 -1.0	± 3.1	457.3	+3.8 -2.8	± 3.2
160	644.0	+0.8 -0.9	± 3.1	404.1	+4.1 -2.8	± 3.1
165	594.0	+0.8 -1.0	± 2.4	375.6	+4.3 -2.7	± 2.6
170	534.3	+0.9 -1.1	± 2.8	340.2	+4.1 -2.9	± 3.0
175	483.9	+1.1 -0.8	± 2.9	308.8	+4.0 -3.1	± 3.1
180	434.5	+1.1 -1.0	± 2.8	278.5	+4.3 -3.3	± 3.0
185	402.8	+1.0 -1.1	± 2.5	256.2	+4.1 -3.3	± 2.6
190	366.0	+0.9 -1.1	± 2.8	233.6	+4.1 -3.3	± 3.0
195	334.6	+0.9 -1.2	± 2.7	214.4	+4.1 -3.4	± 2.9
200	305.5	+1.0 -1.0	± 3.0	196.6	+4.2 -3.5	± 3.1
210	257.0	+0.9 -1.1	± 2.6	165.4	+4.5 -2.9	± 2.6
220	217.5	+1.3 -1.0	± 2.8	140.3	+4.1 -3.2	± 2.9
230	185.9	+1.1 -0.9	± 3.5	119.3	+4.1 -3.1	± 3.6
240	158.9	+1.1 -1.0	± 3.3	101.7	+3.9 -3.0	± 3.4
250	136.8	+0.8 -1.2	± 3.0	86.96	+3.7 -2.9	± 3.2
260	118.3	+0.9 -1.2	± 2.8	74.80	+3.8 -2.6	± 3.1
270	102.8	+1.2 -1.1	± 2.6	64.48	+3.3 -2.5	± 2.8
280	89.49	+1.1 -1.1	± 3.0	55.83	+3.3 -2.4	± 3.2
290	78.61	+1.0 -1.1	± 3.2	48.67	+3.0 -2.2	± 3.2
300	68.86	+1.3 -1.1	± 3.3	42.43	+2.9 -2.2	± 3.6

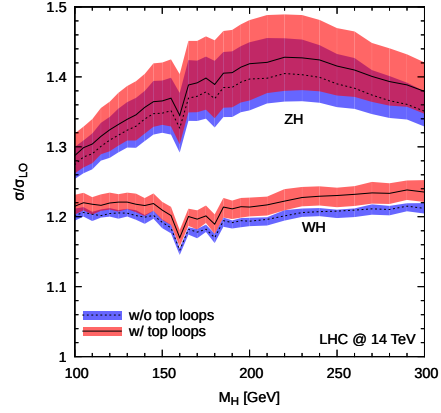
Table 2: Numerical values for the total cross section at LHC at 14 TeV.

M_H [GeV]	$\sigma(WH)$ [fb]	Pert [%]	PDF+ α_s [%]	$\sigma(ZH)$ [fb]	Pert [%]	PDF+ α_s [%]
100	278.0	+4.0 -2.9	± 5.1	161.2	+4.1 -3.0	± 5.5
105	235.7	+4.1 -2.8	± 5.3	138.2	+4.3 -3.0	± 5.6
110	200.9	+4.0 -2.9	± 5.5	119.0	+4.2 -3.1	± 5.7
115	172.1	+4.0 -3.0	± 5.5	103.0	+4.2 -3.1	± 5.8
120	148.0	+4.1 -3.0	± 5.8	89.46	+4.3 -3.2	± 5.9
125	127.5	+4.0 -3.1	± 6.0	77.86	+4.2 -3.2	± 6.1
130	110.2	+4.0 -2.9	± 6.2	67.98	+4.3 -3.1	± 6.0
135	95.61	+4.1 -3.0	± 6.1	59.55	+4.4 -3.2	± 6.0
140	83.06	+4.2 -3.1	± 6.4	52.23	+4.5 -3.3	± 6.2
145	72.36	+4.3 -3.0	± 6.5	46.01	+4.6 -3.2	± 6.3
150	63.16	+4.4 -3.1	± 6.3	40.59	+4.7 -3.3	± 6.0
155	55.28	+4.4 -3.1	± 6.9	35.91	+4.8 -3.3	± 6.6
160	48.49	+4.6 -3.0	± 6.9	31.84	+4.9 -3.3	± 6.5
165	42.54	+4.5 -3.2	± 7.8	28.23	+4.9 -3.4	± 7.3
170	37.51	+4.6 -3.3	± 7.1	25.15	+5.0 -3.5	± 6.6
175	33.26	+4.7 -3.4	± 6.9	22.42	+5.2 -3.6	± 6.4
180	29.53	+4.9 -3.4	± 7.3	20.02	+5.3 -3.6	± 6.6
185	26.29	+4.9 -3.4	± 7.7	17.92	+5.4 -3.7	± 6.9
190	23.39	+5.0 -3.6	± 7.9	16.03	+5.4 -3.8	± 7.0
195	20.86	+5.1 -3.6	± 7.7	14.38	+5.6 -3.9	± 6.8
200	18.61	+5.0 -3.6	± 7.6	12.91	+5.5 -3.9	± 6.5

Table 3: Numerical values for the total cross section at the Tevatron.

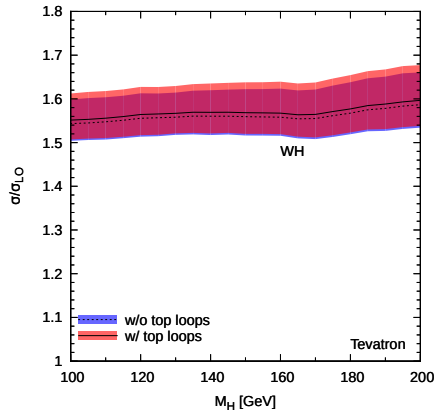


(a)

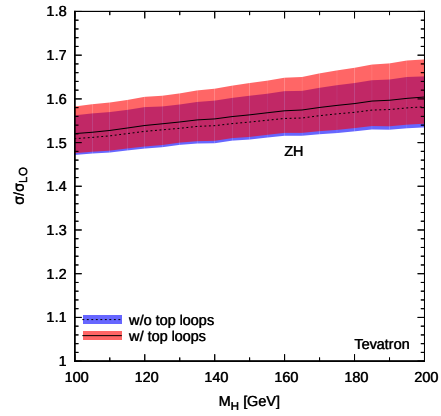


(b)

Figure 8: K-factor at the LHC at (a) 7 TeV and (b) 14 TeV center-of-mass energy, including NNLO QCD and electro-weak corrections, with and without the newly evaluated top-quark induced terms.



(a)



(b)

Figure 9: K-factor at the Tevatron for (a) WH and (b) ZH production, including NNLO QCD and electro-weak corrections, with and without the newly evaluated top-quark induced terms.

Acknowledgments. We would like to thank Stefan Dittmaier and Abdelhak Djouadi for discussions, and Hendrik Mantler for helpful input. RVH and MW thank the CERN PH-TH group for hospitality. This work was supported by *Deutsche Forschungsgemeinschaft*, contract HA 2990/5-1, the Helmholtz Alliance *Physics at the Terascale*, and the Initial Training Network *LHCPhenoNet*.

References

- [1] The ATLAS Collaboration, *Update of the Combination of Higgs Boson Searches in 1.0 to 2.3 fb⁻¹ of pp Collisions Data Taken at $\sqrt{s} = 7$ TeV with the ATLAS Experiment at the LHC*, ATLAS-CONF-2011-135.
- [2] The CMS Collaboration, *Search for standard model Higgs boson in pp collisions at $\sqrt{s} = 7$ TeV and integrated luminosity up to 1.7 fb⁻¹*, CMS PASHIG-11-022.
- [3] R.S. Thorne, G. Watt, *PDF dependence of Higgs cross sections at the Tevatron and LHC: Response to recent criticism*, *JHEP* **1108** (2011) 100, [arXiv:1106.5789](#).
- [4] J. M. Butterworth, A. R. Davison, M. Rubin and G. P. Salam, *Jet substructure as a new Higgs search channel at the LHC*, *Phys. Rev. Lett.* **100** (2008) 242001, [arXiv:0802.2470](#).
- [5] D. Zeppenfeld, R. Kinnunen, A. Nikitenko, E. Richter-Was, *Measuring Higgs boson couplings at the LHC*, *Phys. Rev.* **D 62** (2000) 013009, [hep-ph/0002036](#).
- [6] G. Ferrera, M. Grazzini, F. Tramontano, *Associated WH production at hadron colliders: a fully exclusive QCD calculation at NNLO*, [arXiv:1107.1164](#).
- [7] T. Han and S. Willenbrock, *QCD correction to the pp \rightarrow WH and ZH total cross-sections*, *Phys. Lett.* **B 273** (1991) 167.
- [8] O. Brein, A. Djouadi, R. Harlander, *NNLO QCD corrections to the Higgs-strahlung processes at hadron colliders*, *Phys. Lett.* **B 579** (2004) 149, [hep-ph/0307206](#).
- [9] R. Hamberg, W.L. van Neerven, T. Matsuura, *A complete calculation of the order α_s^2 correction to the Drell-Yan K factor*, *Nucl. Phys.* **B 359** (1991) 343, (E) *ibid.* **B 644** (2002) 403.
- [10] R.V. Harlander and W.B. Kilgore, *Next-to-next-to-leading order Higgs production at hadron colliders*, *Phys. Rev. Lett.* **88** (2002) 201801, [hep-ph/0201206](#).
- [11] S. Dittmaier *et al.* [LHC Higgs Cross Section Working Group Collaboration], *Handbook of LHC Higgs Cross Sections: 1. Inclusive Observables*, [arXiv:1101.0593](#).

- [12] B.A. Kniehl, *Associated Production Of Higgs And Z Bosons From Gluon Fusion In Hadron Collisions*, *Phys. Rev. D* **42** (2253) 1990.
- [13] P.J. Rijken and W.L. van Neerven, *Heavy flavor contributions to the Drell-Yan cross-section*, *Phys. Rev. D* **52** (1995) 149, [hep-ph/9501373](#).
- [14] R.V. Harlander, H. Mantler, S. Marzani, K.J. Ozeren, *Higgs production in gluon fusion at next-to-next-to-leading order QCD for finite top mass*, *Eur. Phys. J. C* **66** (2010) 359, [arXiv:0912.2104](#).
- [15] R.V. Harlander and K.J. Ozeren, *Finite top mass effects for hadronic Higgs production at next-to-next-to-leading order*, *JHEP* **0911** (2009) 088, [arXiv:0909.3420](#).
- [16] S. Marzani, R.D. Ball, V. Del Duca, S. Forte, A. Vicini, *Higgs production via gluon-gluon fusion with finite top mass beyond next-to-leading order*, *Nucl. Phys. B* **800** (2008) 127, [arXiv:0801.2544](#).
- [17] V. Hirschi, R. Frederix, S. Frixione, M.V. Garzelli, F. Maltoni, R. Pittau, *Automation of one-loop QCD corrections*, *JHEP* **1105** (2011) 044, [arXiv:1103.0621](#).
- [18] P. Nogueira, *Automatic Feynman graph generation*, *J. Comp. Phys.* **105** (1993) 279.
- [19] R. Harlander, T. Seidensticker, M. Steinhauser, *Corrections of $\mathcal{O}(\alpha_s)$ to the decay of the Z boson into bottom quarks*, *Phys. Lett. B* **426** (1998) 125, [hep-ph/9712228](#).
- [20] T. Seidensticker, *Automatic application of successive asymptotic expansions of Feynman diagrams*, [hep-ph/9905298](#).
- [21] M. Steinhauser, *MATAD: A program package for the computation of massive tadpoles*, *Comp. Phys. Commun.* **134** (2001) 335, [hep-ph/0009029](#).
- [22] J.A. Vermaseren, *New features of FORM*, [math-ph/0010025](#).
- [23] G. Passarino and M.J.G. Veltman, *One loop corrections for e^+e^- annihilation into $\mu^+\mu^-$ in the Weinberg model*, *Nucl. Phys. B* **160** (1979) 151.
- [24] R. K. Ellis and G. Zanderighi, *Scalar one-loop integrals for QCD*, *JHEP* **0802** (2008) 002, [arXiv:0712.1851](#).
- [25] O. Brein, PhD thesis, *Berlin, Germany: RHOMBOS-Verl. (2003)*.
- [26] G.J. van Oldenborgh and J.A.M. Vermaseren, *New Algorithms for One Loop Integrals*, *Z. Phys. C* **46** (1990) 425.
- [27] FF 2.0, a package to evaluate one-loop integrals, *G.J. van Oldenborgh*, <http://www.xs4all.nl/~gjvo/FF.html>.

- [28] A. Aeppli, *Radiative Corrections in the Electroweak Theory*, Inaugural-Dissertation, Zürich university (1992).
- [29] V.A. Smirnov, *Asymptotic expansions in momenta and masses and calculation of Feynman diagrams*, *Mod. Phys. Lett. A* **10** (1995) 1485, [hep-th/9412063](#).
- [30] V.A. Smirnov, *Applied asymptotic expansions in momenta and masses*, *Springer Tracts Mod. Phys.* **177** (2002) 1.
- [31] R. Harlander, *Asymptotic expansions: Methods and applications*, in *Proc. of the 23rd School of Theoretical Physics (Ustron 99): Recent Developments in Theory of Fundamental Interactions*, Ustron, Poland, 15–22 Sep 1999; *Act. Phys. Pol. B* **30** (1999) 3443, [hep-ph/9910496](#).
- [32] K. Nakamura *et al.* [Particle Data Group Collaboration], *Review of particle physics*, *J. Phys. G* **37** (2010) 075021; <http://pdg.lbl.gov/>.
- [33] S.A. Larin, *The Renormalization Of The Axial Anomaly In Dimensional Regularization*, *Phys. Lett. B* **303** (1993) 113, [hep-ph/9302240](#).
- [34] J. Küblbeck, M. Böhm, A. Denner, *FeynArts: Computer Algebraic Generation Of Feynman Graphs And Amplitudes*, *Comp. Phys. Commun.* **60** (1990) 165. H. Eck, Ph.D. thesis, University of Würzburg (1995); T. Hahn and M. Perez-Victoria, *Automatized one-loop calculations in four and D dimensions*, *Comp. Phys. Commun.* **118** (1999) 153, [hep-ph/9807565](#).
- [35] A. Denner and S. Dittmaier, *Reduction schemes for one-loop tensor integrals*, *Nucl. Phys. B* **734** (2006) 62, [hep-ph/0509141](#).
- [36] A. Denner, S. Dittmaier, *Scalar one-loop 4-point integrals*, *Nucl. Phys. B* **844** (2011) 199, [arXiv:1005.2076](#).
- [37] O. Brein, R.V. Harlander, T.J.E. Zirke, *vh@nnlo: a program to evaluate hadronic Higgs-Strahlung at next-to-next-to-leading order*, (in preparation).
- [38] M.L. Ciccolini, S. Dittmaier, M. Krämer, *Electroweak radiative corrections to associated $W H$ and $Z H$ production at hadron colliders*, *Phys. Rev. D* **68** (2003) 073003, [hep-ph/0306234](#).
- [39] D.L. Rainwater and D. Zeppenfeld, *Searching for $H \rightarrow \gamma\gamma$ in weak boson fusion at the LHC*, *JHEP* **9712** (1997) 005, [hep-ph/9712271](#).
- [40] T. Han, G. Valencia, S. Willenbrock, *Structure function approach to vector boson scattering in pp collisions*, *Phys. Rev. Lett.* **69** (1992) 3274, [hep-ph/9206246](#).
- [41] R.V. Harlander, J. Vollinga, M.M. Weber, *Gluon-Induced Weak Boson Fusion*, *Phys. Rev. D* **77** (2008) 053010, [arXiv:0801.3355](#).

- [42] P. Bolzoni, F. Maltoni, S.O. Moch, M. Zaro, *Higgs production via vector-boson fusion at NNLO in QCD*, *Phys. Rev. Lett.* **105** (2010) 011801, [arXiv:1003.4451](#).
- [43] P. Bolzoni, F. Maltoni, S.-O. Moch, M. Zaro, *Vector boson fusion at NNLO in QCD: SM Higgs and beyond*, [arXiv:1109.3717](#).